The net force acting on the cylinder may be obtained by solving Eq. (1) for the pressure and integrating around the surface of the cylinder. However, since the cylinder represents a closed curve, the $\Pi(t)$ term will contribute nothing to this integration and the hydrostatic pressure term gh will contribute only a constant buoyant force. Moreover, the $q^2/2$ term is symmetrical about the y-axis and, consequently, will yield no net contribution to the x-component of force. We are left, therefore, with

$$-\rho\partial\phi/\partial t \tag{2}$$

as the only term in the expression for pressure which will contribute to a horizontal component of force. Thus, the x and y components of inertial force exerted on the circular cylinder may be written as

$$X = -\oint_c P dy = \rho\partial/\partial t \oint_c \phi dy \tag{3}$$

and

$$Y = \oint_c P dx = -\rho\partial/\partial t \oint_c \phi dx \tag{4}$$

respectively. (It may be noted that the $q^2/2$ term is not symmetrical with respect to the x-axis and, therefore, a lift force proportional to velocity squared does exist.)

Combining Eqs. (3) and (4)

$$-Y + iX = \rho\partial/\partial t \oint_c \phi dz \tag{5}$$

where the complex number z is defined as $z = x + iy$. Since the stream-function is constant (or zero) on the surface of the cylinder we may write Eq. (5) as

$$-Y + iX = \rho\partial/\partial t \oint_c w(z) dz \tag{6}$$

where the complex potential is defined as $w(z) = \phi + i\psi$ and ϕ and ψ denote the velocity potential and stream function, respectively.

The complex potential for flow past a circular cylinder touching a plane boundary as depicted in Fig. 1 is given by Milne-Thomson[2] as

$$w(z) = a\pi U \coth(a\pi/z) \tag{7}$$

where a denotes the radius of the cylinder and U the free-stream velocity. Using this expression, Eq. (6) becomes

$$-Y + iX = \pi a\rho\dot{U} \oint_c \coth(a\pi/z) dz \tag{8}$$

where the integration is to be carried out around the closed curve C representing the surface of the cylinder. However, since $w(z)$ is an analytic function, we may apply Cauchy's integral theorem to the region bounded by the closed curve C representing the cylinder, the x-axis and the arc of radius R as labeled C_∞ in Fig. 2. Accordingly, the integral represented in Eq. (8) may be expressed as the sum of the integrals along the various segments of the complete contour as

$$\int_c = \int_{c_1} + \int_{c_2} + \int_{c_\infty} \tag{9}$$

It may be noted that $\cosh(\pi a/z)$ is analytic throughout the region bounded by the lines C, C_1, C_2 and C_∞. However, since $\coth(\pi a/x)$ is an odd function about $x = 0$ the integrals along C_1 and C_2 cancel each other leaving

$$-Y + iX = \pi\rho a\dot{U} \oint_{c_\infty} \coth(\pi a/z) dz \tag{10}$$

where the integration is to be carried out along the semicircular arc labeled C_∞ in Fig. 2.

In order to evaluate the integral occurring in Eq. (10) we write $z = Re^{i\theta}$ and expand the integrand for large values of R. This gives,

$$\coth(a\pi/z) = (R/a\pi)[1 + \tfrac{1}{3}(a\pi/R)^2 e^{-i2\theta} + O(1/R^4)]e^{i\theta}, R \to \infty \tag{11}$$

Substituting Eq. (11) into Eq. (10) and carrying out the integration gives the x and y components of inertial force as

$$Y = 0 \tag{12}$$

$$X = \rho\pi a^2\dot{U}(\pi^2/3) \tag{13}$$

where the inertial force is defined as positive in the positive x-direction, i.e., in the direction of the acceleration of the ambient fluid. According to the usual definitions of added mass and inertial coefficients, we have

$$C_I \equiv X/\pi a^2\rho\dot{U} \equiv 1.0 + C_m \tag{14}$$

Accordingly, the added mass coefficient is given as

$$C_m = \pi^2/3 - 1.0 = 2.29 \tag{15}$$

It may be noted that Dalton and Helfinstine's value of $C_m = 2.22$ is only slightly in error when compared to the exact value as given in Eq. (15).

Conclusions

The exact solution for the added mass coefficient for a circular cylinder in contact with a plane boundary has been developed. The value of $C_m = 2.29$ so obtained is shown to be considerably larger than the value of $C_m = 1.0$ for a circular cylinder in an infinite fluid. The proximity of the rigid boundary has the effect of increasing the value of the added mass coefficient. The results are of particular interest in the calculation of wave forces on bottom mounted structures such as pipelines and submerged tanks.

References

[1] Dalton, C. and Helfinstine, R. A., "Potential Flow Past a Group of Circular Cylinders," *ASME* Paper 71–FE–18, 1971.

[2] Milne-Thomson, L. M., *Theoretical Hydrodynamics*, 4th ed., Macmillan, New York, 1960, p. 174.

Mean Velocity Profiles for Turbulent Shear Flow

R. E. Powe,* H. W. Townes,† and J. L. Gow‡
Montana State University, Bozeman, Mont.

In any investigation of either turbulent boundary-layer flow or enclosed turbulent flow, it is necessary to utilize some known expression for the mean velocity profile. One manner by which such an expression is commonly obtained is through the use of a three-layer scheme which divides the flowfield into three regions—a wall region, a buffer zone, and a turbulent core. The mean velocity profile expressions utilized with this model are given by Schlichting[1] to be

$$\bar{U}/u^* = yu^*/\nu \quad \text{for} \quad yu^*/\nu \leq 5 \tag{1a}$$

$$\bar{U}/u^* = 5.0 \ln(yu^*/\nu) - 3.05 \quad \text{for} \quad 5 \leq yu^*/\nu \leq 30 \tag{1b}$$

$$\bar{U}/u^* = 2.5 \ln(yu^*/\nu) + 5.5 \quad \text{for} \quad yu^*/\nu \geq 30 \tag{1c}$$

Received August 16, 1971.

* Assistant Professor. Aerospace and Mechanical Engineering Department.

† Associate Professor. Aerospace and Mechanical Engineering Department.

‡ Presently at Hurlbut, Kersich, and McCullough Consulting Engineers, Billings, Mont.

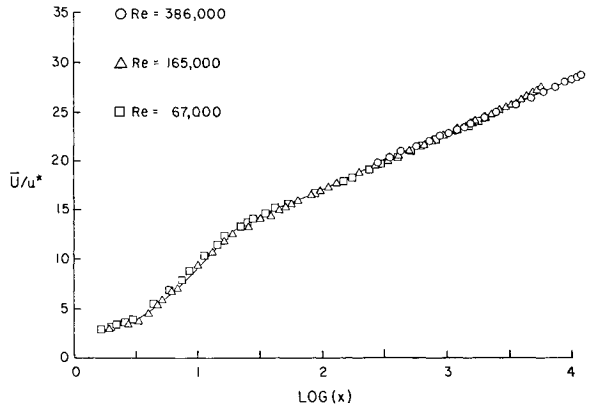

Fig. 1 Logarithmic mean longitudinal velocity profiles.

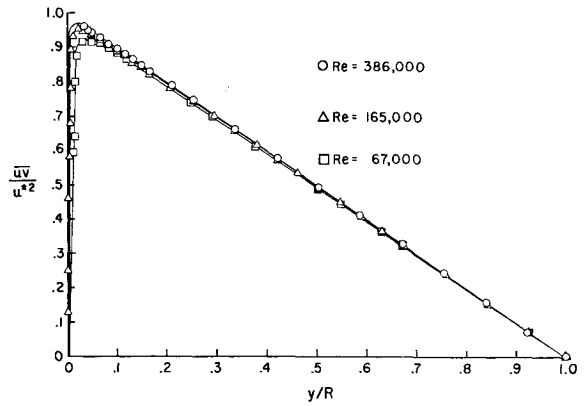

Fig. 3 Comparison of measured and predicted values of the Reynolds stress for turbulent pipe flow.

where $\bar{U}$ is the mean velocity component, u^* is the shear velocity, ν is the kinematic viscosity, and y is the distance from the solid boundary.

However, it is also well known that Eqs. (1) cannot be theoretically correct since they do not yield a continuous velocity gradient, nor do they satisfy the appropriate boundary condition at large distances from the boundary. Although such deviations are not critical in some applications, they are of utmost importance in others. For instance, one quantity of interest in many turbulence applications is the eddy diffusivity for momentum which can be calculated from the Reynolds stress, and the Reynolds stress can be determined from the mean velocity gradient normal to the solid boundary. Therefore, for such an application it is desirable to have available a mean velocity profile expression which is theoretically plausible. Such an expression was developed by the authors during the course of an investigation of turbulent pipe flow.

This expression was obtained by modifying and combining two previously proposed relations for different regions of the pipe. Kays[2] has shown that the equation

$$\bar{U}/u^* = a \ln(x) + b \quad \text{for} \quad x \geq x_0 \tag{2}$$

not only allows for a slight Reynolds number dependence but also yields a zero velocity gradient at the pipe centerline in contrast with Eq. (1c). The parameter x in Eq. (2) is an indication of location defined as

$$x = [3yu^*(2 - y/R)]/[2\nu(3 - 4y/R + 2y^2/R^2)] \tag{3}$$

where R is the pipe radius. Longwell[3] indicates that the equation

$$\bar{U}/u^* = c \tanh(x/c) \quad \text{for} \quad x \leq x_0 \tag{4}$$

satisfies the wall boundary conditions and yields continuity in the velocity and its gradient at x_0, the point where this equation is matched with a relationship for the center region of the pipe. The empirical constants appearing in Eqs. (2) and (4) have not been previously determined.

During the course of the current investigation, the data of Gow[4] and Powe[5] for Reynolds numbers between 50,000 and 500,000 were curve fit in order to determine these quantities. Using data from 25 different mean velocity profile runs, a, b, c, and x_0 were found to be 2.42, 5.98, 14.68, and 27.75, respectively. Equations (2) and (4) are compared with the commonly used, three layer model, Eqs. (1), in Fig. 1. Also shown in this figure are representative data for small, medium, and large Reynolds numbers. An error analysis for the approximately 500 data points utilized in obtaining the empirical constants revealed an average deviation from Eqs. (2) and (4) of only 2.4%, while 98% of these data were within ±10% of the equations. Thus, Eqs. (2) and (4) appear to represent a universal velocity profile relationship, as shown in Fig. 2, and have the advantage over previously proposed relationships of satisfying all boundary conditions as well as the Reynolds equations.

Once a velocity profile expression is available, the longitudinal Reynolds equation, as given by Laufer,[6] can be used to calculate the $\overline{uv}$ Reynolds stress, where u and v represent longitudinal and radial fluctuating velocity components. The results of such calculations are compared in Fig. 3 with experimentally determined values of the Reynolds stress, and excellent agreement is noted for all Reynolds numbers.

The eddy diffusivity for momentum is defined by Schlichting[1] as

$$\epsilon = -\overline{uv}/(d\bar{U}/dy) \tag{5}$$

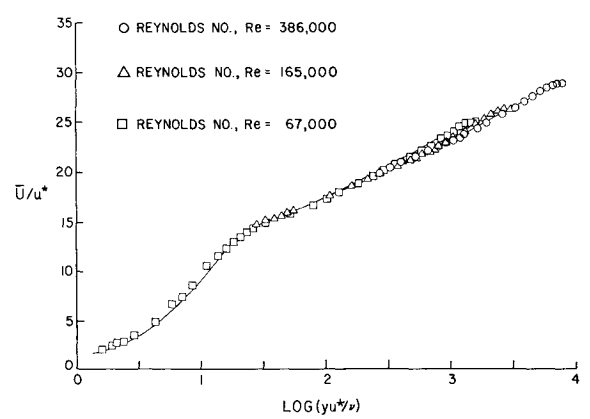

Fig. 2 Universal longitudinal mean velocity profile.

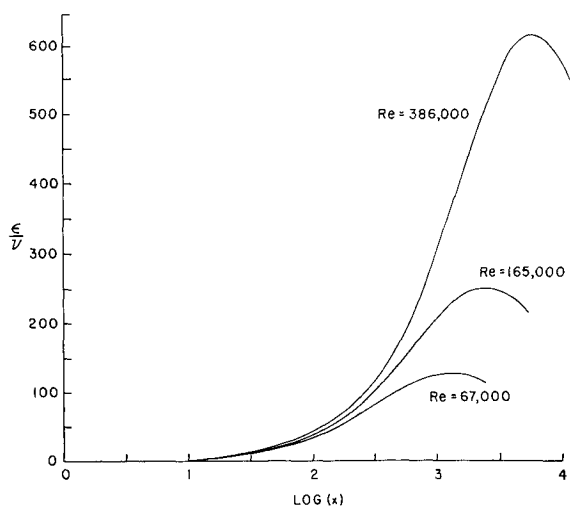

Fig. 4 Eddy diffusivity for momentum predicted from universal velocity profile expression.

and values of this quantity may now be calculated. Such results for three different Reynolds numbers are indicated in Fig. 4.

In summary, this note has presented a mean velocity profile expression for turbulent flow which is apparently universal in nature. This expression was obtained by modifying and combining two previously proposed expressions for different regions of the flowfield. Values of the Reynolds stress, and of the eddy diffusivity for momentum, obtained using these expressions were presented for Reynolds numbers from 50,000 to 500,000.

References

[1] Schlichting, H., *Boundary Layer Theory*, McGraw-Hill, New York, 1968, Chaps. 19–20.

[2] Kays, W. M., *Convective Heat and Mass Transfer*, McGraw-Hill, New York, 1966, p. 71.

[3] Longwell, P. A., *Mechanics of Fluid Flow*, McGraw-Hill, New York, 1966, p. 325.

[4] Gow, J. L., *Fully-Developed Turbulent Flow in Smooth and Rough-Walled Pipe*, M. S. thesis, 1969, Mechanical Engineering Dept., Montana State Univ., Bozeman, Mont.

[5] Powe, R. E., *Turbulence Structure in Smooth and Rough Pipes*, Ph.D. thesis, 1970, Aerospace and Mechanical Engineering Dept., Montana State Univ., Bozeman, Mont.

[6] Laufer, J., "The Structure of Turbulence in Fully-Developed Pipe Flow," Rept. 1174, 1954, NACA.

Effects of a Flexible Surface on Surface Shear-Stress Fluctuations beneath a Turbulent Boundary Layer

MICHAEL E. MCCORMICK*, BRUCE JOHNSON†, AND WILLIAM M. LEE‡

U.S. Naval Academy, Annapolis, Md.

Nomenclature

C	= elastic wave velocity
f	= frequency
P	= pressure
Q	= quality factor
$U(y)$	= flow velocity
U_c	= convection velocity
y	= normal coordinate to plate
α	= angle of incidence
β	= damping factor
δ	= boundary-layer thickness
τ	= shear stress
ω_1	= circular fundamental frequency
$\langle\ \rangle$	= mean value

Introduction

THE study of turbulent boundary-layer induced vibrations of plates and membranes is most significant in understanding the production of near field sound generated by submerged bodies. In addition to the self-noise problems, this area of study is relevant to the phenomenon of drag reduction by compliant surfaces.

Although the nature of the pressure fluctuations on a surface beneath a turbulent boundary-layer and the behavior of associated excited surfaces are rather well understood,[1–3] the effect of surface compliance on the time-dependent surface shear stress has not been adequately investigated. The significance of such an investigation is that the shear stress fluctuation beneath a turbulent boundary-layer is a local phenomenon and, therefore, not significantly influenced by radiation.

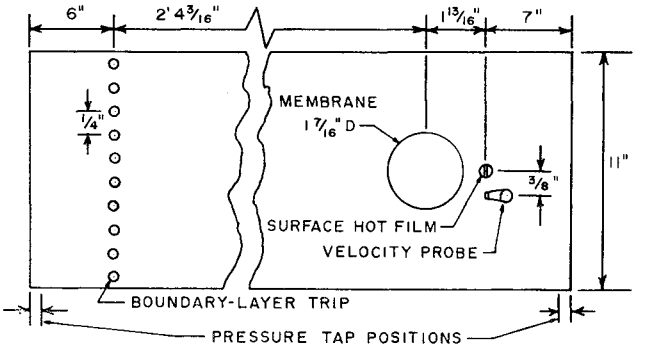

Fig. 1 Schematic diagram of the top of the experimental apparatus.

In the present study, a circular membrane is flush-mounted in the surface of a flat plate which is inclined at a negative angle of attack in a low-turbulence subsonic wind tunnel. The boundary-layer over the plate is turbulent due to the presence of trips mounted well upstream of the membrane. The effect of motions of the membrane on the fluctuating surface shear stress is studied by placing a flush-mounted hot-film just downstream of the membrane. The motions of the center of the membrane are measured using a fiber-optic displacement probe.

Experimental Apparatus

An aluminum membrane of 0.00005 in. thickness was stretched over the opening of a $1\frac{7}{16}$ in. i.d. steel tube and mounted in a flat plate as shown in Fig. 1. The plate was mounted in a low-turbulence subsonic wind tunnel at a negative angle of incidence of 3° as shown in Fig. 2. The sides of the plate were lined with foam rubber and pressed against the tunnel side-walls to prevent edge flows. Static pressure taps were located in the tunnel walls above the leading and trailing-edges of the plate to measure the pressure gradient over the plate. Studs $\frac{1}{16}$ in. in height and $\frac{3}{16}$ in. in diameter were situated 6 in. from the leading edge to insure the existence of a turbulent boundary-layer. The centers of the studs were separated by $\frac{1}{4}$ in.

A thermo-systems hot-film velocity probe was mounted $\frac{3}{8}$ in. downstream of the membrane as shown in Figs. 2 and 3. The height of the probe was adjustable so that the velocity profile in the boundary-layer could be measured. The surface shear stress fluctuations were measured using a thermo-systems flush-mounted hot-film probe as shown in Figs. 2 and 3. This probe is $\frac{3}{32}$ in. in diameter with a platinum film mounted on a flat head.

Motions of the center of the membrane were measured using a MTI Fotonic Sensor which is a fiber-optic probe $\frac{1}{8}$ in. in diameter. This probe was mounted $\frac{3}{32}$ in. from the static equilibrium position of the membrane, see Fig. 3. Leads from the probes were enclosed in a fairing beneath the plate.

Signals from the probes were amplified and recorded on a Hewlett-Packard 4-channel tape recorder. A schematic dia-

Table 1 Flow data

Run	P(in. H_2O)	δ(in.)	U(fps)	$\langle U^2\rangle/U_\delta$	$R_\delta(\times 10^{-4})$
1	0.063	0.500	30.5	0.0850	0.747
2	0.137	0.468	58	0.0664	1.250
3	0.195	0.437	68.5	0.0505	1.547
4	0.378	0.406	83.4	0.0414	1.745
5	0.484	0.375	122	0.0284	2.400

* Associate Professor of Ocean Engineering and Chairman, Dept. of Naval Systems Engineering.

† Professor of Ocean Engineering.

‡ Associate Professor of Mechanical Engineering.